KSCE Journal of Civil Engineering (2021) 25(1):256-271
DOI 10.1007/s12205-020-0548-6

pISSN 1226-7988, eISSN 1976-3808
www.springer.com/12205

Structural Engineering

Correlation Study between Seismic Intensity Measures and Nonlinear Response of Arch Dam via Endurance Time Analysis

Chao Liang[a], Jianyun Chen[b], Qiang Xu[a], and Jing Li[c]

[a]*Institute of Earthquake Engineering, Dalian University of Technology, Dalian 116024, China*
[b]*State Key Laboratory of Coastal and Offshore Engineering, Dalian University of Technology, Dalian 116024, China*
[c]*Faculty of Infrastructure Engineering, Dalian University of Technology, Dalian 116024, China*

ARTICLE HISTORY

Received 26 March 2020
Accepted 2 August 2020
Published Online 26 October 2020

KEYWORDS

Endurance time analysis method
Seismic intensity measures
Nonlinear response of high arch dam
Correlation
Sufficiency

ABSTRACT

Predicting the structural response efficiently and quickly is a major focus in civil engineering. For concrete dams, due to the structure's complexity, it is difficult to obtain the structural performance timely through a large number of calculations. In this paper, the relationship between structural responses and seismic intensity mesures (IMs) is established under the framework of endurance time analysis method (ETAM) with its good accuracy and high efficiency. Baihetan arch dam is selected as a case study, and the dam-reservoir-foundation system is excited under fourteen sets of endurance time acceleration functions (ETAFs) which are generated through the response spectra of ground motion records. The results show that, compared with displacement-dependent damage indices (DIs), damage-dependent DIs can better reflect damage characteristics of the arch dam under different damage levels. Among the ETA-related IMs, the combined spectral acceleration is the most practical and proficient, followed by acceleration spectral intensity (ASI) and effective peak acceleration (EPA). For high arch dam, the influence of the higher order modes should be fully taken into account when establishing the correlation between the structural response and the IMs. The sufficiency of IMs based on structural response should also be fully demonstrated.

1. Introduction

Predicting the structural response given certain earthquake condition has always received great attention in recent years. This is not only very important in performance-based seismic engineering (PBEE) (Alavi and Krawinkler, 2001), but also very crucial in structural vulnerability assessment (Hariri-Ardebili and Saouma, 2016a). In order to establish the perfect relationship between structural response and intensity measures (IMs) successfully, it is very important to identify the optimal IM which sufficiently correlates with structural response. Many IMs have been used to predict the structural damage level effectively. These IMs can be divided into two categories: structure-specific IMs and non-structure-specific IMs (Kostinakis et al., 2018). An optimal seismic intensity parameter should satisfy practicality, efficiency, sufficiency and scaling robustness (Luco and Allin, 2007; Padgett et al., 2008; Mehanny, 2009). Among the IM's characteristics mentioned above, effectiveness is usually used to determine the superiority of IMs. An effective IM can improve the accuracy of structural response assessment, so it requires a smaller number of nonlinear time history analyses to obtain an ideal result.

At present, incremental dynamic analysis (IDA) is often considered as an effective method to acquire structural dynamic nonlinear responses. However, IDA often requires a lot of nonlinear dynamic time history analysis with low computational efficiency, especially for large complex structures with the high nonlinearity of materials and the complexity of structural models. It is obvious that for complicated structures, such as concrete dams, performing a great quantity of nonlinear analyses under different excitation levels (and, finally, extracting and summarizing the results) is nearly impossible for practitioners (Hariri-Ardebili and Saouma, 2016c). Endurance time analysis method (ETAM) is a dynamic pushover method which combines with the advantages of pushover analysis and IDA (Estekanchi et al., 2004). It assumes that the structure is subjected to pre-

CORRESPONDENCE Chao Liang ✉ lcsg6213@mail.dlut.edu.cn Institute of Earthquake Engineering, Dalian University of Technology, Dalian 116024, China

designed intensifying excitation called endurance time acceleration function (ETAF) (Riahi et al., 2009). These simulated acceleration functions shake the structure from a low excitation level (the structural response within the elastic range) to a high excitation level (leading to failure). Therefore, the trend of structure performance with seismic intensity measures can be obtained by ETAM. At present, ETAM has been applied to many types of structures, such as steel structures (Estekanchi et al., 2011), steel liquid storage tanks (Estekanchi and Alembagheri, 2012), shell structure (Tavazo et al., 2012), highway bridges (Guo et al., 2017).

Several researches have also been carried out in terms of concrete dams via ETAM. Hariri-Ardebili and his collaborators has investigated the seismic response of a high arch dam subjected to a set of real ground motions and generic ETAFs. These publications referred to the linear (Hariri-Ardebili and Mirzabozorg, 2011) and nonlinear behavior of the same arch dam with concrete smeared crack (Hariri-Ardebili and Mirzabozorg, 2014) and discrete crack in the vertical and peripheral joints (Hariri-Ardebili et al., 2014). Overall, the application of the ETAM was satisfactory compared to the multiple time history analysis (MTHA). Meghella and Furgani (2014) and Furgani and Meghella (2015) showed other aspects of the ETAM on Italian arch dams. Again, results confirm that ETA is as good as time history analysis (THA), and it more rapidly characterizes the performance curves. Later, a series of performance and damage indices for arch dams (Hariri-Ardebili et al., 2016) is proposed and applied on an arch dam with concrete damage plasticity model. Similarly, for gravity dams, several studies (Valamanesh et al., 2011; Salamon et al., 2019) have also demonstrated the efficiency of ETAM compared with traditional time-history analysis. The results show that the results of ETA and THA were in good agreement for all responses, and ETAM can predict the outcome of multiple dynamic time analyses with good accuracy and high efficiency. To sum up, it is found that, for concrete dams, especially arch dams studied, ETAM can provide a quite reliable safety assessment by processing only part of ETAFs.

In the present paper, the relationship between structural responses and seismic intensity measures is established under the framework of ETAM. Considering its applicability and efficiency, ETAM can provide a new idea for establishing the relationship between structural responses and seismic intensity parameters efficiently and quickly, and it can also provide a reference for rapid seismic performance evaluation, seismic failure mode analysis of structures and optimization of ETAF generation. On the other hand, ETAFs adopted in this paper satisfy the dispersion of response spectra of actual ground motions, and they are based on the characteristics of response spectra of actual ground motions, which is different from other studies.

This paper is organized as follows. Section 2 introduces sixteen ETA-related IMs and two categories of seismic damage indices of high arch dam. The detailed description on the finite element numerical model and the selection, input of ground motions is introduced in Section 3. In Section 4, a dam-reservoir-foundation system is excited under fourteen sets of endurance time acceleration functions (ETAFs) which are generated through the response spectra of selected ground motion records. Then the ETA results are further analyzed and evaluated using probabilistic approaches. Based on the analysis results, the distribution characteristics of each IM under ETAFs are given, and the relationship between each IM and the structural response is established. Compared with the previous studies on the structural response of arch dams, the classification of damage level is used to show the evolution of structural damage in this paper. Finally, the probabilistic seismic demand model (PSDM)'s parameters are used to evaluate the IMs related to structural response. Section 5 presents the conclusion.

2. Background Theory

2.1 Endurance Time Analysis

2.1.1 Characteristics of ETAFs

The generation of an ETAF can be summarized as follows (Estekanchi et al., 2007; Nozari and Estekanchi, 2011):

The ETAF requires that for an accelerogram, the target response spectrum with the duration time t is defined by

$$S_{aT}(T,t) = \frac{t}{t_{Target}} S_{aC}(T), \tag{1}$$

$$S_{uT}(T,t) = \frac{t}{t_{Target}} S_{aC}(T) \times \frac{T^2}{4\pi^2}, \tag{2}$$

where $S_{aT}(T, t)$, $S_{uT}(T, t)$ is the target acceleration response spectrum and the displacement response spectrum at time t, respectively. t_{Target} is the target time that is fixed to scale the accelerogram. T is the period of free vibration and $S_{aC}(T)$ is a pre-specified response spectrum (generally the codified design acceleration spectrum or the response spectrum generated by ground motion).

In order to find an accelerogram that satisfies the target response defined by Eqs. (1) and (2), an unconstrained optimization problem in the time domain is as follows:

$$\min F(\ddot{u}_g) = \int_0^{T_{\max}} \int_0^{t_{\max}} \left\{ \left[S_a(T,t) - S_{aT}(T,t) \right]^2 + \alpha \left[S_u(T,t) - S_{uT}(T,t) \right]^2 \right\} dt dT, \tag{3}$$

where $\ddot{u}_g$ is the ETAF to be sought and α is a relative weight that can adjust the effective penalty owe to displacement deviation relative to acceleration deviation from target values (Estekanchi et al., 2007). Also, $t_{\max}$ is duration of ETAFs, and $T_{\max}$ is the maximum period to be considered during the generation. $S_a(T,t)$ and $S_u(T,t)$ is the acceleration response and displacement response value for period T at time t. In this paper, the acceleration response spectrum is selected as the target spectrum, that is, α is taken as 0. The key to generate an ETAF is how to find an optimal ground motion time history, $\ddot{u}_g$, so that its response spectrum and the target response spectrum can be maximally matched at any time. The unconstrained optimization problem here is solved by lsqnonlin function in the MATLAB optimization toolbox (Matlab,

2016). The selection of initial input accelerogram has a great influence on the efficiency of the optimization algorithm. In order to improve the efficiency of optimization iteration, an initial input accelerogram that gradually increases with time is generated according to the target acceleration response spectrum. The duration of ETAF is set to be 30 seconds. Then 3000 points are discretized in the range of 0 – 30 seconds on the time scale uniformly, and 300 points are discretized in the range of 0 – 6 seconds on the periodic scale logarithmically. Considering that the maximum peak acceleration of the nonlinear analysis of the arch dam is 1.2 g in the authors' research group (Chen et al., 2020a; Chen et al., 2020b), and that the adopted input profile function is a linear profile, the target time of the series of ETAFs is set to 10s to make the arch dam have strong nonlinearity in 30 seconds. That is, the peak acceleration of ETAFs from 0 to 10s is 0.4 g.

2.1.2 Seismic Intensity Measures Related to ETAF

Similar to the general ground motion time history, the ETA-related IMs can be also divided into non-structure-specific IMs and structure-specific IMs. In this paper, a total of 16 seismic parameters are considered, including peak ground acceleration (PGA), cumulative absolute velocity (CAV), Arias intensity (I_A), characteristic intensity (I_c), acceleration spectral intensity (ASI), effective peak acceleration (EPA), spectral acceleration at first-natural period ($S(T = T_1, \xi = 5\%)$), spectral acceleration of specific modes ($S(T = T_i, \xi = 5\%)$, $i = 2, 3, 4, \ldots, 5$), multiple-period intensities ($S_a^{1\text{-to-}N}$, N =2, 3, 4, 5).

Table 1 presents an overview of the used parameters and the corresponding references, where $a(t)$ refers to the time history of ground motion, t_{tot} refers to the ground motion duration (here refers to specific duration of ETAF), g is gravity acceleration, a_{RMS} is the root-mean-square of acceleration, α_i is the ratio of effective masses, and m_i^{eff} is the effective masses for the ith mode. Also, N is the number of the effective modes, and j is the number of the first mode involved in the summation operation, and is generally taken as 1.

2.2 Seismic Damage Indices

2.2.1 Displacement-Dependent DIs

In this paper, the maximum absolute values of displacements relative to the dam heel at crown cantilever crest is considered, as defined below:

$$DI_{displacement}(t) = \Omega(\Delta(t)) - \Delta_{ini}, \tag{4}$$

where $\Omega(\Delta(t))$ refers to the maximum absolute values of displacements relative to the dam heel at crown cantilever crest up to t, Δ_{ini} is the initial (dead weight + hydrostatic pressure) response.

Table 1. Seismic Intensity Parameters

IM	Equation or defination	Application or description	References
Peak ground acceleration (PGA)	$PGA = \max(\lvert a(t)\rvert)$	Widely used in hazard maps and attenuation relations.	(Kramer, 1996)
Cumulative absolute velocity (CAV)	$CAV = \int_0^{t_{tot}} \lvert a(t)\rvert dt$	Best correlates with the onset of damage.	(Kramer, 1996)
Arias intensity (I_A)	$I_A = \frac{\pi}{2g}\int_0^{t_{tot}} (a(t))^2 dt$	A measure of the total energy content of seismic excitation.	(Arias, 1970)
Characteristic intensity (I_c)	$I_c = (a_{RMS})^{3/2}\sqrt{t_{tot}}$, $a_{RMS} = \left(\frac{1}{t_{tot}}\int_0^{t_{tot}} (a(t))^2 dt\right)^{1/2}$	An index of structural damage due to maximum deformations and absorbed hysteretic energy.	(Ang, 1990)
Acceleration spectral intensity (ASI)	$ASI = \int_{0.1}^{0.5} S_a(T, \xi = 5\%) dt$	Characterize strong ground motion for analysis of concrete dams.	(von Thun et al., 1988)
Effective peak acceleration (EPA)	$EPA = \frac{1}{2.5} \times \frac{\int_{0.1}^{0.5} S_a(T, \xi = 5\%) dt}{0.4}$	The average acceleration response spectrum within the period range of 0.1 to 0.5s, divided by a standard value 2.5.	(BSSC, 1984)
Effective peak acceleration at dam bedrock (EPA_{dam})	$EPA_{dam} = S_a(0.2, \xi = 5\%)/2.5$	The ground motion parameters related to the dam site in the western United States.	(Chen et al., 2012)
Spectral acceleration at first-natural period	$S(T = T_1, \xi = 5\%)$	T_1 is the first-natural period of the structure, and ξ refers to the damping ratio.	-
Spectral acceleration of specific modes	$S(T = T_i, \xi = 5\%)$, $(i = 2,3,4,\ldots,5)$	Account for the higher-order vibration modes, where T_i is the period of the ith mode.	-
Multiple-period intensities	$S_a^{1-to-N} = \Sigma_{i=1}^{N}(S(T_i, \xi = 5\%))^{\alpha_i}$, $\alpha_i = \frac{m_i^{eff}}{\Sigma_j^N m_i^{eff}}, i = 2,3,4,5$	Primarily used for high-rise building structures and accounts for both the higher-order modes and the effective mass at each mode.	(Hariri-Ardebili and Saouma, 2016b)

2.2.2 Damage-Dependent DIs

In this paper, the plastic-damage model (Lee and Fenves, 1998) is used to simulate the damage cracking behavior of concrete dam under ground motions. To quantify the damage degree of concrete arch dam under ground motions, the damage volume ratio is defined as

$$DI_{volume,d=dt} = \frac{V_{d=dt}}{V_0}, \tag{5}$$

where V_0 is the volume of arch dam, $V_{d=dt}$ is the proportion of dam body with the damage factor greater than d_t (d_t = 0.0, 0.3, 0.5, 0.8). $DI_{volume,d=dt}$ can indicate the damage range of the dam under different damage levels.

Similarly, we can also propose the damage area ratio, as defined below:

$$DI_{area,d=dt} = \frac{A_{d=dt}}{A_0}, \tag{6}$$

where $A_{d=dt}$ is the damage area at time t, A_0 is the total area of dam. This DI can be calculated for both the upstream and downstream faces, denoted as $DI^{upstream}_{area,d=dt}$ and $DI^{downstream}_{area,d=dt}$ respectively, which can describe the damage state of the dam surface.

2.3 Probabilistic Seismic Demand Model

PSDMs can offer a statistical relationship between structural response and seismic intensity measures. According to the work by Cornell et al. (2002), the probabilistic seismic demand model can be represented by lognormal distribution.

$$P[D \geq d|IM] = 1 - \Phi\left(\frac{In(d) - In(S_D)}{\beta_{D|IM}}\right) \tag{7}$$

where $\Phi(\cdot)$ is the standard normal cumulative distribution function, S_D and $\beta_{D|IM}$ is the median value and the logarithmic standard deviation of the structural demand on condition of the IM, respectively. It was found that S_D and IM can be thought to satisfy the following relationship:

$$S_D = aIM^b. \tag{8}$$

So if we take the logarithm of Eq. (8), we can get

$$In(S_D) = b \cdot In(IM) + In(a), \tag{9}$$

where a and b are regression coefficients, which can be obtained from linear regression of nonlinear time history analyses. Besides, the conditional standard deviation of the regression, $\beta_{D|IM}$ is given by

$$\beta_{D|IM} \cong \sqrt{\frac{\sum\left(In(d_i) - In\left(aIM^b\right)\right)}{N-2}}, \tag{10}$$

where d_i is the ith structural demand from the nonlinear time history analyses, and N is the number of nonlinear transient analyses.

Based on the above model, the correlation between structural response and seismic intensity parameters can be measured from four aspects, as listed in Table 2.

3. Model and Ground Motions

Structural analysis is carried out using a commercial finite element software (Simulia, 2011), in which concrete was modeled by a damage-plasticity model (Lee and Fenves, 1998; Pan et al., 2009; Wang et al., 2013b), and contraction joint opening is considered in a highly nonlinear system. The radiation damping of semi-infinite bedrock is simulated by the 3D infinite element model (Simulia, 2011; Mirzabozorg et al., 2012; Hariri-Ardebili et al., 2014) in the investigation. Several complex methods have been used to model the dam–water interaction (Camara, 2000; Wang et al., 2013a), but there generally exists a low computational efficiency for vast calculations of high arch dams, particularly when PSDM is used to evaluate the structural performance. Therefore, added

Table 2. Criteria for an Optimal IM

Criteria for an optimal IM	Defination and description
Efficiency	A more efficient IM can yield less dispersion about the estimated demand median, showing a lower $\beta_{D\|IM}$ (Eq. (10)), which is inversely proportional to efficiency.
Practicality	Practicality is used to check whether or not there is any direct correlation between an IM and the structural demand. Practicality is measured by b in Eq. (9). A high value of b is indicative of increased practicality.
Proficiency	Proficiency is evaluated by ζ, (the lower the value of ζ is, the higher proficiency is).
Sufficiency	Sufficiency is evaluated by the [a]p-value. Higher p-value means more sufficient IM than other seismic hazard characteristics [b](M or R).

Note: The efficiency or practicality alone often causes conflicting conclusions. In order to trade-off the effects of different measure indicators, proficiency combines the characteristics of the efficiency and practicality. By substituting Eq. (9) into Eq. (7), we can yield:

$$P[D \geq d|IM] = \Phi\left(\frac{In(IM) - In(a)}{\frac{\beta_{D|IM}}{b}}\right), \text{so } \zeta = \frac{\beta_{D|IM}}{b}$$

[a]Numerically p-values are obtained from linear regression of the residuals, $\varepsilon|\text{IM}$, from the PSDM relative to the ground motion characteristic, M or R (Luco and Cornell, 2007).
[b]M and R are the magnitude and epicentre distance of an earthquake event, respectively.

mass technique (Westergaard, 1933; Kuo, 1982; National Energy Administration of China, 2015) is suggested to model the hydrodynamic pressure.

3.1 Dam Finite Element Model

A double curvature arch dam, Baihetan arch dam, is taken as the analytical model. The dam consists of the main body, the concrete pedestal at the left bank and the concrete spread foundation at the bottom of the dam. The dam foundation and crest are at 545 m and 834 m above sea level, respectively. The dam is composed of 11 blocks, with a total crest length of 727 m and the crown cantilever thickness ranging from 63.5 m at the base to 14 m at the crest. The normal water level is 825 m. Figs. 1(a) and 1(b) shows the finite-infinite element coupling model and 10 contraction joints, respectively. The finite element is surrounded by infinite elements (Simulia, 2011). The ground motions are transformed into the equivalent nodal force acting on the coupling interface nodes between infinite and finite elements. On the input method of ground motion for infinite element dynamic boundary, see reference (Song et al., 2018) for a detailed derivation. The whole finite element model consists of 33708 solid elements and 39243 nodes. The positive directions in the global coordinates (X, Y, Z) are from the left bank to the right bank, from the upstream to downstream, and from bottom to top, respectively.

To simulate the behaviour of shear keys set in the contraction joint, tangential springs with high rigidity is simulated between the joints of the contact surface to prevent the contraction joint from sliding (Buffi et al., 2017; Omidi and Lotfi, 2017). For simplicity, a sufficiently large value for the tangential spring is given (Zhang et al., 2009). In addition, a contact surface model that conforms to Eqs. (11) and (12) is used to simulate the opening and closing of the contraction joints between adjacent portions.

$$p = 0 \text{ for } h < 0 \tag{11}$$

$$p > 0 \text{ for } h = 0 \tag{12}$$

where p and h are the contact pressure and the overclosure between the contact surfaces, respectively. The pressure-overclosure relationship curve is shown in Fig. 1(e).

3.2 Material Parameters

According to the partition design of concrete materials, the whole dam body is divided into three major zones, as shown in Fig. 1(c). The material parameters of each zone are summarized in Table 3. It is assumed that the dynamic strength for mass concrete is 20% higher than the static strength, and the dynamic tensile strength is 10% of the dynamic compressive strength, according to Chinese specifications (National Energy Administration of China, 2015). And the dynamic tensile strength and dynamic compression strength are given in this table.

Figure 1(d) illustrates the constitutive relation of concrete, namely the damage-plasticity model (Lee and Fenves, 1998; Pan et al., 2009; Wang et al., 2016; Omidi and Lotfi, 2017), where σ

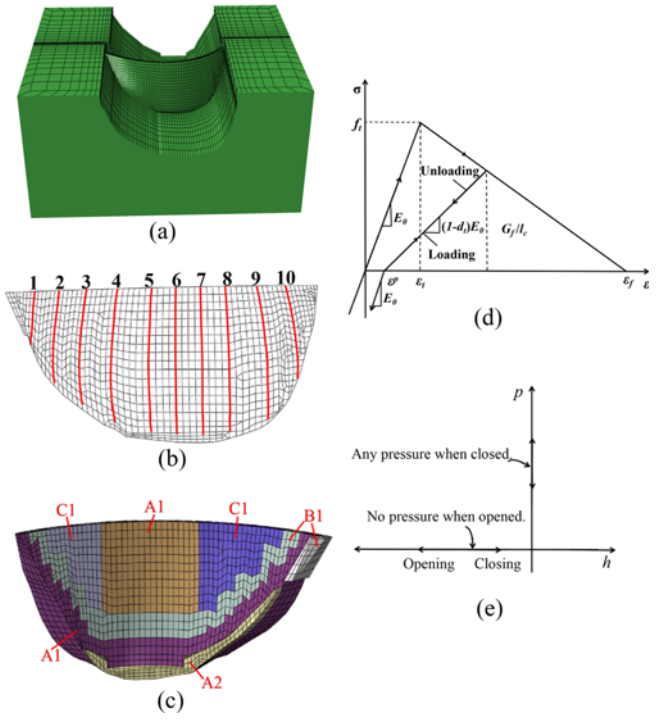

Fig. 1. Dam-Reservoir-Foundation System and Constitutive Model: (a) Dam Foundation System, (b) Dam Contraction Joints, (c) Dam Partitions, (d) The Constitutive Relation of Concrete, (e) The Pressure-Overclosure Relationship Curve

and ε represent the stress and strain of concrete, respectively; E_0 is the initial elastic modulus of concrete; d_t represents the tensile damage factor varying from 0 (elastic status) to 1 (completely damaged status); G_f represents the fracture energy of concrete; f_t represents the tensile strength of concrete; ε_t and ε_f represent the maximum elastic strain and ultimate tensile strain of concrete, respectively; and l_c represents the characteristic length (0.45 m here) of concrete. It is assumed that the damping type of the concrete arch dam is rayleigh type with 5% damping ratio for the first and sixth modes. The calculated mass-proportional coefficient and stiffness-proportional coefficient are 0.6395 s^{-1} and 0.0035 s, respectively.

3.3 Ground Motion Characteristics

3.3.1 Selection and Processing of Ground Motion Records

Ground motions at a specific site suffer significant repercussions from hypocenter, transmission, and local site conditions. Combined with the seismic risk analysis of the dam site, three factors are considered in the selection of records: 1) earthquake magnitude (5.0 – 8.0); 2) hypocentral distance (0 – 100 km); and 3) rock site (shear wave velocity, $V_{S30} \geq 800$ m/s). Finally, fourteen groups of three-component records are selected from the PEER strong ground motion database (PEER, 2013), as listed in Table 4. The response spectra of horizontal and vertical ground motions are shown in Fig. 2, where the vertical site spectra are 2/3 of the

Table 3. Mechanical Properties of Concrete and Rock

Materials	Zones	Modulus of elasticity	Mass density	Poisson's ratio	Tensile strength	Compressive strength	Fracture energy	Maximum crack strain
		(E_c, GPa)	(ρ_c, kg/m^3)	ν_c	(f_t, MPa)	(f_c, MPa)	(G_f, N/m)	($\varepsilon_f \times 10^{-6}$)
Concrete	A1and A2	32.5	2,400	0.167	3.834	38.409	341	395
	B1	31.5	2,400	0.167	3.414	34.15	303	394
	C1	30.0	2,400	0.167	2.974	29.808	264	395
Rock	Foundation	26.0	2,800	0.245	-	-	-	-

Table 4. Selected Three-Component Seismic Ground Motion Records

Record sequence number	Earthquake name	Station name	Year	Magnitude	Epicenter distance (km)	V_{S30} (m/s)
RSN23	San Francisco	Golden Gate Park	1957	5.28	11.02	874.72
RSN4312	Umbria-03_ Italy	Gubbio	1984	5.6	15.72	922
RSN680	Whittier Narrows-01	Pasadena - CIT Kresge Lab	1987	5.99	18.12	969.07
RSN703	Whittier Narrows-01	Vasquez Rocks Park	1987	5.99	50.39	996.43
RSN804	Loma Prieta	So. San Francisco_ Sierra Pt.	1989	6.93	63.15	1020.62
RSN1091	Northridge-01	Vasquez Rocks Park	1994	6.69	23.64	996.43
RSN1108	Kobe_ Japan	Kobe University	1995	6.9	0.92	1043
RSN1245	Chi-Chi_ Taiwan	CHY102	1999	7.62	37.72	804.36
RSN1347	Chi-Chi_ Taiwan	ILA063	1999	7.62	61.06	996.51
RSN1518	Chi-Chi_ Taiwan	TCU085	1999	7.62	58.09	999.66
RSN2508	Chi-Chi_ Taiwan-03	CHY102	1999	6.2	60.36	804.36
RSN2929	Chi-Chi_ Taiwan-04	TTN042	1999	6.2	69	845.34
RSN3318	Chi-Chi_ Taiwan-06	CHY102	1999	6.3	63.26	804.36
RSN4083	Parkfield-02_ CA	PARKFIELD - TURKEY FLAT #1 (0M)	2004	6	5.29	906.96

horizontal site spectra. It is seen that these response spectra is near to the site response spectrum.

3.3.2 The Generation of ETAFs

Firstly, the response spectra of the selected records are calculated as the target response spectra of ETAFs, and then the corresponding ETAFs are generated according to the ETAF program. Finally, these ETAFs are grouped into 14 groups according to station names of ground motion records, each containing two horizontal and one vertical direction. And the correlation coefficient among three directions for each group of ETAFs is less than 0.2. Fig. 3 shows the three-component ETAFs and the corresponding to acceleration response spectra for RSN2909 record. In any given period of time, the response spectrum of the ETAF is proportional to the target one, i.e. the response spectrum at t =10s is twice the intensity of the spectrum at t = 5s, half the intensity at t = 20s and

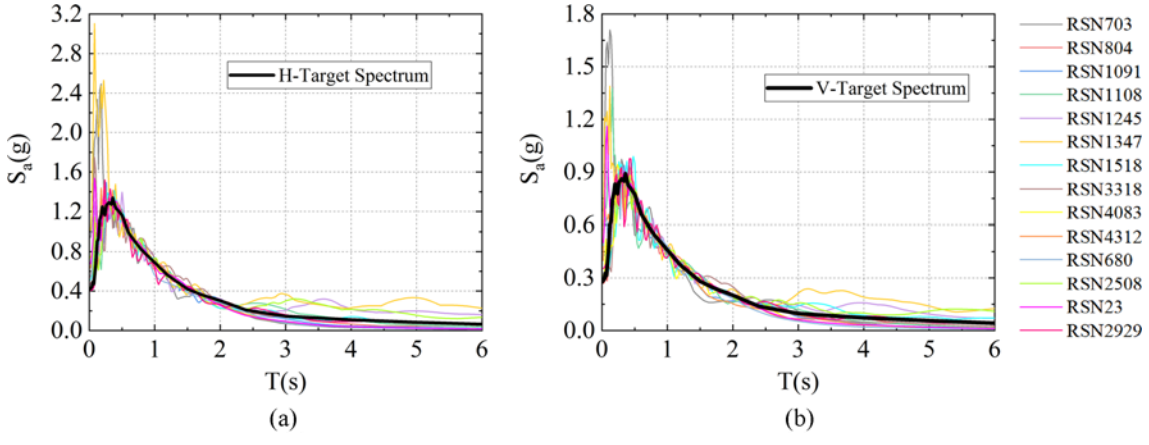

Fig. 2. Matching Results of Response Spectrum and Target Spectrum: (a) Horizontal Direction, (b) Vertical Direction

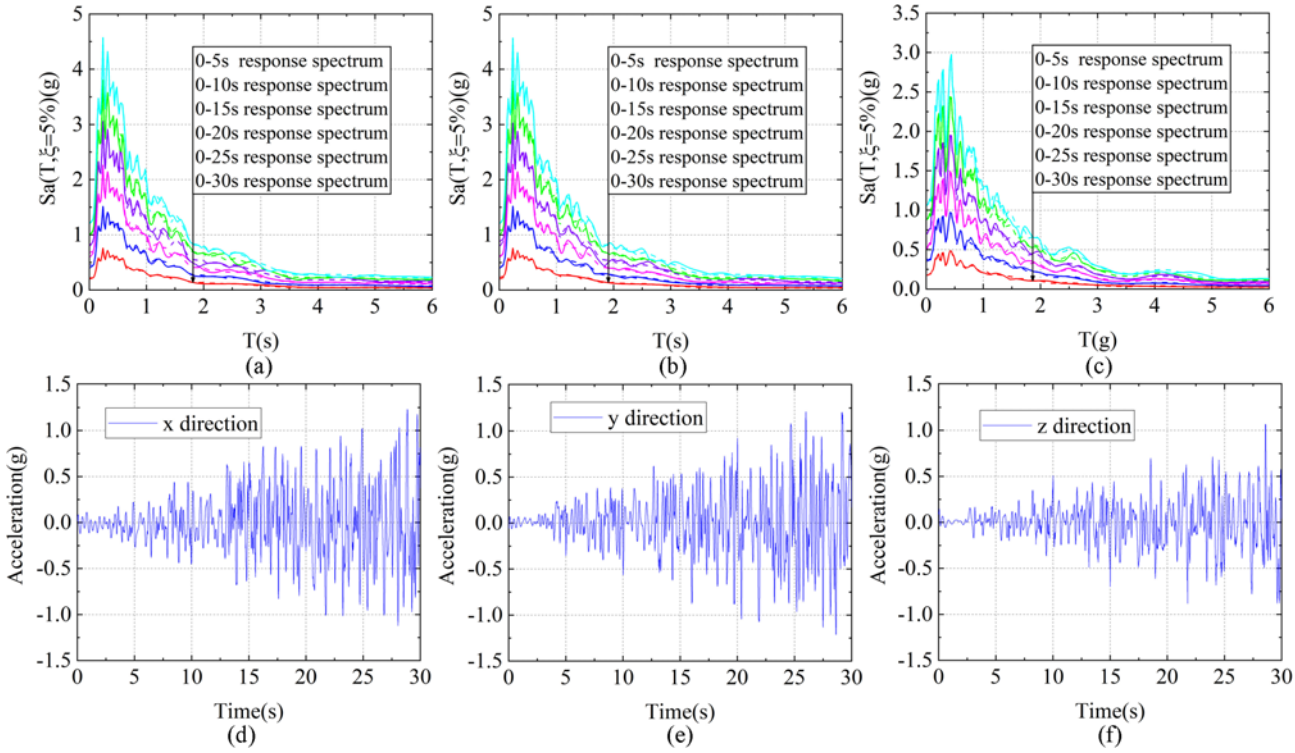

Fig. 3. Characteristics of a Set of ETAFs for RSN2909 Record: (a) x-Direction ETAF, (b) y-Direction ETAF, (c) z-Direction ETAF, (d) x-Direction Response Spectrum, (e) y-Direction Response Spectrum, (f) z-Direction Response Spectrum

a third the intensity at t = 30s.

3.3.3 Applied Loads and Dynamic Analysis

The dynamic time history analysis of Baihetan arch dam is conducted by the ETAM in the present paper. The loads considered in the analysis include: 1) dead weight and hydrostatic pressure, and 2) seismic excitation. The whole dam-foundation-water system is excited by three-component ETAFs with its combination of 100%X, 100%Y and 66.7%Z based on Chinese specifications (National Energy Administration of China, 2015).

4. Results and Discussion

4.1 Endurance Time Analysis Curve

In order to build the correlation between the seismic intensity measures and the structural responses, we need to do one-step processing for the response time histories obtained by ETAM. ETA Curve is plotted for each response of arch dam, in which its ordinate's values represent the maximum response absolute values during the time interval from 0.0 to t based on Eq. (13):

$$\Omega\left(f\left(t\right)\right) \equiv Max\left(Abs\left(f\left(\tau\right):\tau \in \left[0,t\right]\right)\right), \tag{13}$$

where Ω acts as the maximum absolute operator, $f(t)$ represents time-history of the considered response parameter, τ refers to the dummy variable for time.

Figure 4(a) shows an example for the generation of ETA curve, while ETA curves for $DI_{displacement}$ under all sets of ETAFs is depicted in Fig. 4(b). It can be seen that the ETA curve shows great discreteness, so it is necessary to summarize and quantify such data to obtain the general statistical law. For $DI_{displacement}$, their (16, 50 and 84%) fractile curves are graphically depicted in Fig. 4(c).

Similarly, we can also get ETA curves and fractile curves of $DI_{volume,d=dt}$ and $DI_{area,d=dt}$, as shown in Figs. S1 – S3, respectively. It is obvious that these ETA curves can be divided into three stages: 1) the first stage that $DI_{volume,d=dt}$ or $DI_{area,d=dt}$ is 0.0, showing that there occurs no such damage, 2) the second where $DI_{volume,d=dt}$ or $DI_{area,d=dt}$ is gradually increasing, and 3) the final stage where macro-crack appears (when damage level is greater than 0.8, we generally believe that there occurs macro-cracks in the dam body.). The three stages are divided as shown in Fig. 4(d). For ETA curves of $DI_{volume,d=dt}$ (d_t = 0.0, 0.3, 0.5, 0.8) under RSN2508 Record, $DI_{volume,d=0.8}$ has just occurred at 15.44 s, but $DI_{volume,d=0.0}$ has reached 1.0 at this time, and $DI_{volume,d=0.3}$ and $DI_{volume,d=0.5}$ has a new turning point. The three stages of other damage indices are basically similar to this case. In contrast to $DI_{displacement}$, $DI_{volume,d=dt}$ and $DI_{area,d=dt}$ can better reflect the stage of structural damage development.

Further, the corner points and slope after corner points for ET curves of different damage indices are statistically analyzed in this paper. It is worth mentioning that the corner point here refers to the moment that damage indices start gradually increasing, while the slope after corner point here refers to the average slope from the corner point of ETA curve to the moment that there

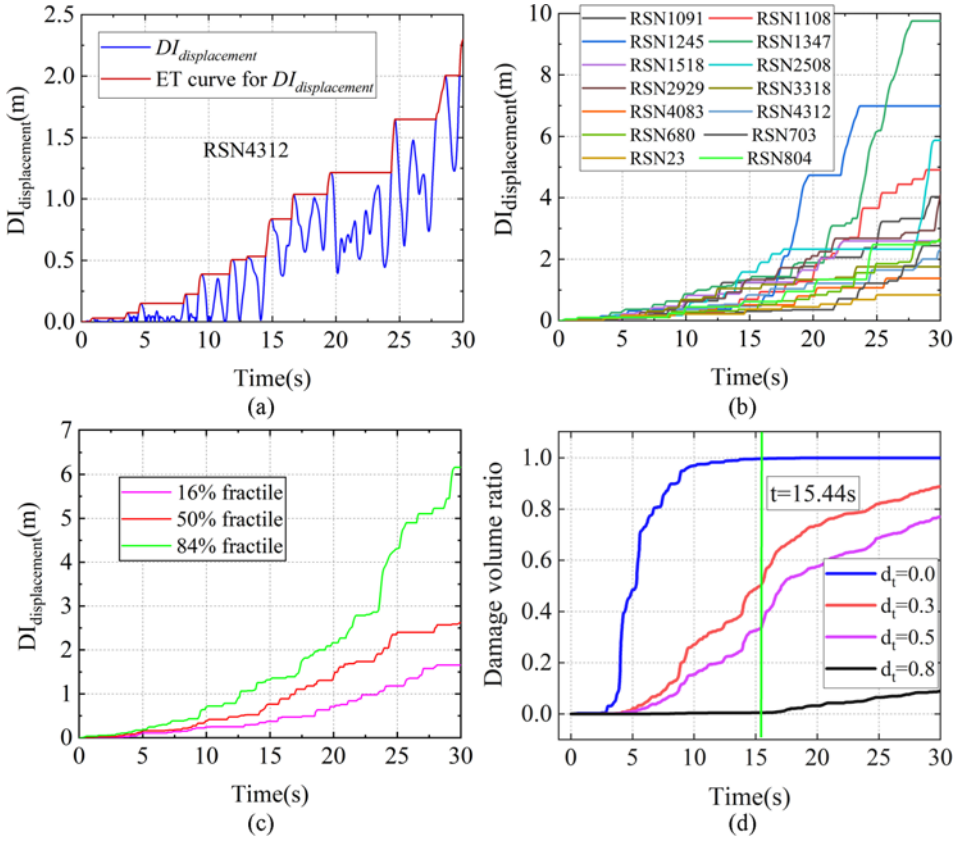

Fig. 4. Time Histories and ETA Curves: (a) Time-History and ETA Curve of $DI_{displacement}$ for RSN4312, (b) ET Curves of $DI_{displacement}$ for All Sets of ETAFs, (c) Their Summary (16, 50 and 84%) Fractile Curves, (d) ET Curves of Different Damage Level for Record #RSN2508

occur macro-cracks in the dam body. The data are fitted through the normal distribution model. The shapiro-wilk (SW) test (Razali and Wah, 2011) is used to investigate whether the data obey a normal distribution. The test statistic, W, ranges from 0 to 1. Small values of W causes rejecting normality, while a value of 1 means normality of the data. The levels of significance, α = 5%, is considered and the results are shown in Table S1.

Figures S4 – S6 show the histograms and distributional models of the corner points and slopes for ET curves of different damage levels, and the corresponding distribution parameters are shown in Fig. 5. It is obvious that the corner points and slopes of ET curves with different damage levels obey normal distribution at α = 5%. As the damage level increases, the mean value (MV) of corner points in the corresponding ET curves also increases, but the MV of the slopes after the corner point decreases, while the MVs of corner point and the corresponding slope with damage level greater than 0.3 are close to those with the damage level greater than 0.5. This means that when the damage levels are 0.3 and 0.5, the overall development trends of arch dams are basically similar. In addition, when the damage level is less than 0.8, the standard deviations (SDs) of the corner points corresponding to the ET curves also increase with the increase of the damage level, whereas the SDs of the slopes after the corner points decrease except the development of $DI_{area,d=dt}^{upstream}$.

4.2 The Establishment of IMs vs. DIs

Since seismic intensity measures are often used to evaluate and express the structural seismic performance, it is necessary to convert time to seismic intensity measures to improve the efficiency of the ETA curves. Therefore, a correlation between time in ETAM and the IMs should be found.

Figrue 6 shows the varying curves of different IMs with time in ETAM. It is worth mentioning that these IMs are directly computed by ETAF along the river due to less correlation coefficient among three components. It can be seen that these IMs show obvious variability, which mainly comes from the variability of ETAF target spectrum. In addition, the ground motion intensity parameters can be mainly divided into two categories: 1) one directly related to the response spectra of ETAFs, which shows a linear increase trend with time, and is directly calculated by the response spectra of ETAFs, corresponding to the feature of ETAFs (that is, the response spectra of ETAFs increase linearly with time); 2) another directly related to ETAFs, which shows a curve increase trend with time, and is calculated by ETAFs. Compared with the first type of IMs, the energy accumulation of the ground motion process is considered for the second type of IMs and the variation is also related to duration. The first type of IMs is mainly studied in the present paper.

Next, the relationship between DIs and IMs are determined,

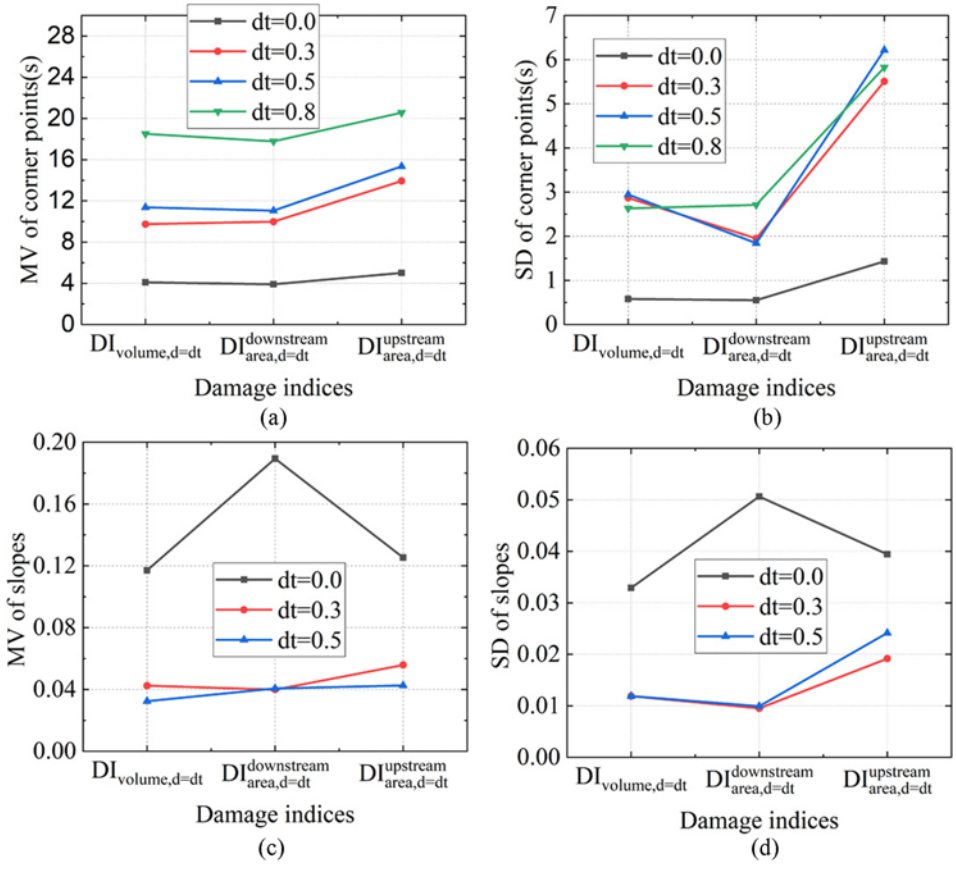

Fig. 5. Distributed Parameter Statistics of Corner Points and Slopes under Different Damage Levels: (a) Mean Value (MV) of Corner Points, (b) Standard Deviation (SD) of Corner Points, (c) Mean Value (MV) of Slopes after Corner Points, (d) Standard Deviation (SD) of Slopes after Corner Points

and results are plotted on a cartesian coordinates (Figs. 7(a) – 7(d)) and logarithmic coordinates (Figs. 7(e) – 7(h)), e.g., $DI_{displacement}$ vs. $S(T = T_1, \xi = 5\%)$, $DI_{displacement}$ vs. PGA, $DI_{volume,d=0.0}$ vs. $S(T = T_1, \xi = 5\%)$ and $DI_{volume,d=0.0}$ vs. PGA. These scatter data points show linear trend in the logarithmic coordinates, while they show a power curve in the cartesian coordinates.

The scatter plots of $S(T = T_i, \xi = 5\%)$ versus DIs (e.g., $DI_{displacement}$, $DI_{volume,d=0.0}$) in the logarithmic coordinate are further given in Fig. 8. It is worth mentioning that the scatter plots of other seismic intensity parameters and DIs are similar to above scatter plots. So the results can be used to develop a PSDM which is a relationship between DIs and IMs, as described in Section 2.3.

4.3 Optimal IM Selection

4.3.1 Based on Displacement-Dependent DIs

Now let us research the correlation between $DI_{displacement}$ and IMs first. Evaluation is made according to the four criteria in Section 2.3. The evaluation indicators of each IM are shown in Table 5.

Practicality is assessed from b. On the whole, the slope of the combined spectrum acceleration is much larger than those of other IMs, and the slope increases with the increase of combined modes. Clearly there is no obvious difference among five spectral accelerations (T_1 to T_5), and those IMs related to a specific vibration period of dam have a slope in the range of 1.43 – 1.50. In addition, ASI and EPA are defined to integrate the acceleration response spectrum in the periodic range of 0.1 – 0.5s, including a large range of specific vibration periods of the structure, so their slopes are larger than the spectral acceleration of the specific vibration period of the structure. For IMs calculated directly by ETAFs, except PGA, the slope of I_c, I_A and CAV are smaller.

Efficiency is gauged by β, (the lower, the better). It can be seen that for the combined spectral acceleration with higher order modes, the deviation decreases with the increase of the combined modes, and the value of β is in the range of 0.62 – 0.70. However, there is no obvious regularity for the spectral acceleration associated with a specific vibration period of dam. The value ranges from 0.59 to 0.72, where $S(T = T_3, \xi = 5\%)$ is the largest and $S(T = T_5, \xi = 5\%)$ is the smallest. For IMs calculated directly by ETAFs, I_c, I_A and CAV except PGA, the value of β is also smaller.

Proficiency is evaluated by ζ, (the lower the value of ζ is, the higher proficiency is). For the combined spectral acceleration, the value of ζ is between 0.08 and 0.23, which is much smaller

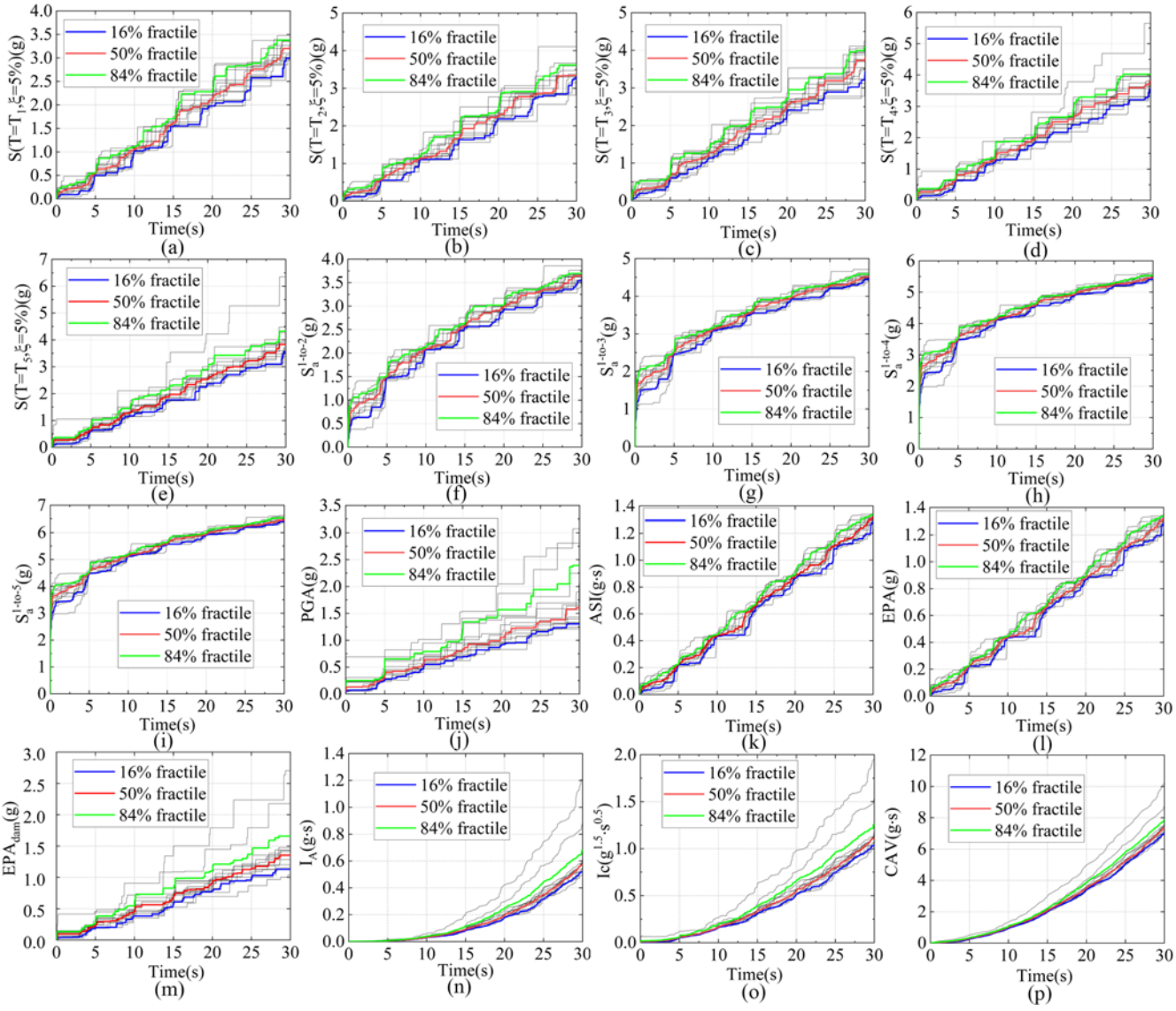

Fig. 6. Correlation between Time and IMs: (a) $S(T = T_1, \xi = 5\%)$, (b) $S(T = T_2, \xi = 5\%)$, (c) $S(T = T_3, \xi = 5\%)$, (d) $S(T = T_4, \xi = 5\%)$, (e) $S(T = T_5, \xi = 5\%)$, (f) $S_a^{1\text{-to-}2}$, (g) $S_a^{1\text{-to-}3}$, (h) $S_a^{1\text{-to-}4}$, (i) $S_a^{1\text{-to-}5}$, (j) PGA, (k) ASI, (l) EPA, (m) EPA_{dam},, (n) I_A, (o) I_c, (p) CAV

than those of other IMs, and the value decreases as higher modes is combined. For the spectral acceleration associated with the specific vibration period of the arch dam, the value ranges from 0.4 to 0.5. The value of ζ corresponding to EPA and ASI is smaller than the spectral acceleration with a specific vibration period. The seismic intensity parameter calculated directly from ETAF has a significantly larger ζ value, with a maximum of 0.79 for I_A and a minimum of 0.44 for PGA.

Goodness-of-fitting (GOF) is often used to evaluate the quality of data fitting. The IMs associated with ETAFs listed in this paper basically have higher R^2 values with a range of 0.79 – 0.88. By contrast, the combined spectral acceleration still shows an obvious regularity. As the number of modes increases, the R^2 value increases, and the corresponding range is 0.83 – 0.86. Among the remaining IMs, CAV is the largest and EPA_{dam} is the smallest.

In total, combined spectra acceleration, $S_a^{1\text{-to-}N}$, are the most practical and proficient in whole set. Peak ground acceleration (PGA) and the spectral acceleration with a specific vibration period have no obvious advantages in this paper, though they always are widely used in performance-based seismic design. In fact, as a complex structure, the seismic response of arch dam is not simply related to the spectral acceleration of a particular mode of the structure. It can be reflected from ASI, EPA and the combined spectral acceleration, which include several specific vibration periods of structure. From the results shown in Table 5, ASI and EPA are the same results. This is mainly because their expressions are similar, although their definitions are different. Since I_c, I_A and CAV do not reflect the characteristics of the structure, they seem to be worse than other IMs. The sufficiency about PGA and the spectral acceleration corresponding to a particular vibration period is studied in Section 4.4.

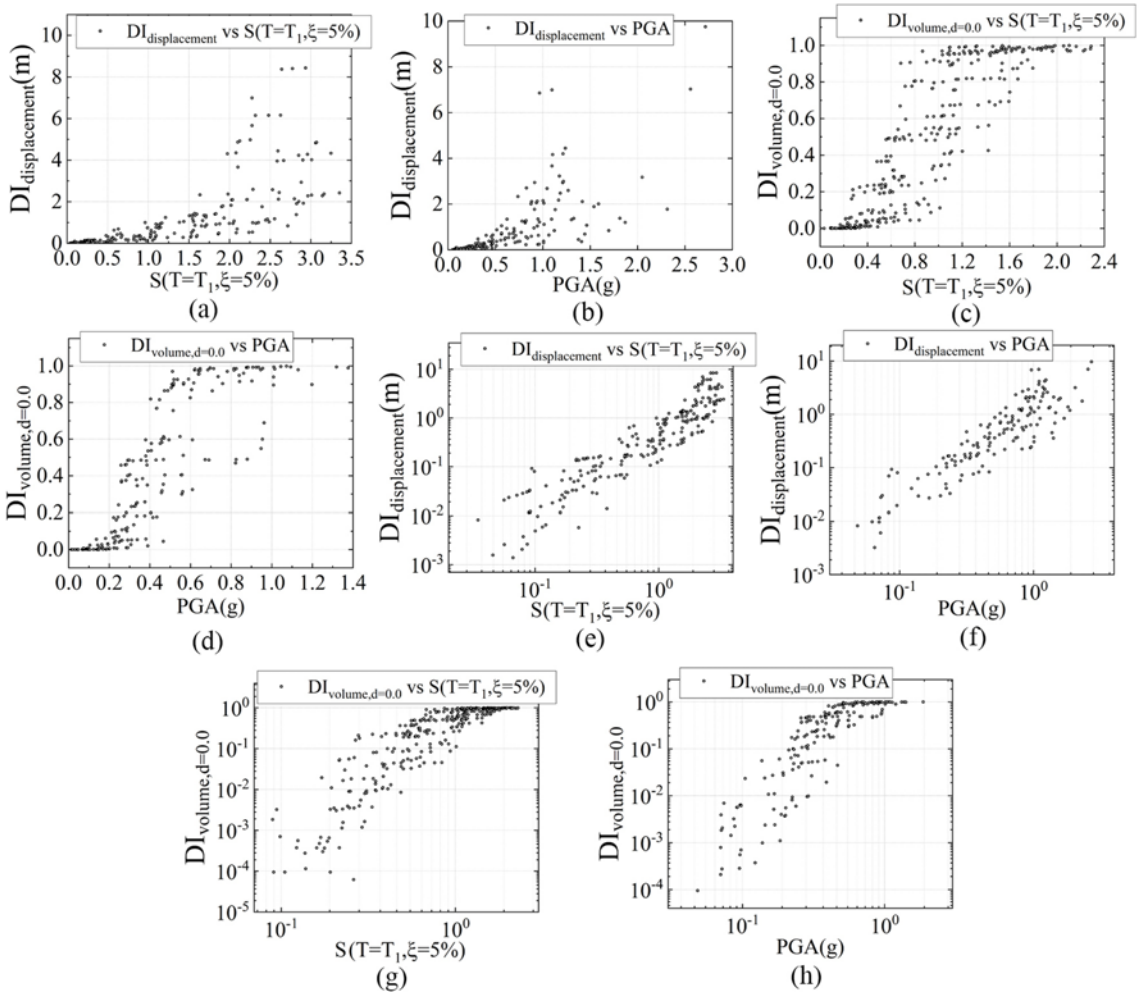

Fig. 7. EDPs-IMs Results: (a) $DI_{displacement}$ vs. $S(T = T_1, \xi = 5\%)$, (b) $DI_{displacement}$ vs. PGA, (c) $DI_{volume,\ d=0.0}$ vs. $S(T = T_1, \xi = 5\%)$, (d) $DI_{volume,\ d=0.0}$ vs. PGA in Arithmetic Scale, (e) $DI_{displacement}$ vs. $S(T = T_1, \xi = 5\%)$, (f) $DI_{displacement}$ vs. PGA, (g) $DI_{volume,\ d=0.0}$ vs. $S(T = T_1, \xi = 5\%)$, (h) $DI_{volume,\ d=0.0}$ vs. PGA in Logarithmic Scale

4.3.2 Based on Damage-Dependent DIs

The correlation between IMs and damage-dependent DIs is further studied. The corresponding PSDM's parameters are shown in Fig. 9. It is evident that the combined acceleration response spectra, $S_a^{1\text{-}to\text{-}N}$, are also the most practical and proficient, and peak ground acceleration (PGA) and the spectral acceleration with a specific vibration period still have no obvious advantages compared with other IMs. However, the practicality of IMs to the damage-dependent DIs is generally stronger than that of the displacement-dependent DIs, although the corresponding deviation is larger. In addition, for displacement response, PGA has higher proficiency than $S(T{=}T_1, \xi{=}5\%)$, while for damage-dependent DIs, $S(T{=}T_1, \xi{=}5\%)$ is generally higher proficiency than PGA. It is concluded that the correlation of the IMs to different structural response parameters is different.

Specifically, the practicality of $DI_{area,d=dt}^{downstream}$ to IMs is stronger than these of $DI_{volume,d=0.0}$ and $DI_{area,d=dt}^{upstream}$ when damage level is higher ($d_t = 0.3$ and $d_t = 0.5$), and its deviation is smaller; while the practicality of $DI_{area,d=dt}^{upstream}$ to most of IMs (especially ones directly related to the response spectra of ETAFs) is slightly stronger than these of $DI_{volume,d=0.0}$ and $DI_{area,d=dt}^{downstream}$ under lower damage level ($d_t = 0.0$), although is deviation is larger. Therefore, under lower damage level ($d_t = 0.0$), the upstream damage area ratio slightly has higher proficiency; under higher damage level ($d_t = 0.3$ and $d_t = 0.5$), the downstream damage area ratio has higher proficiency.

4.4 IMs' Sufficiency Based on Structural Response

In this section, IMs' sufficiency (including PGA and spectrum accelerations with different modes, $S(T = T_i, \xi = 5\%)$, $i = 2,3,4, \ldots, 5$) is studied. The research method is detailed in Section 2.3. Unlike that, spectrum accelerations with different modes are selected as seismic hazard parameters (Abrahamson and Silva, 1997; Garcia-Mayordomo and Insua-Arevalo, 2011; Zacchei and Molina, 2020) rather than M_w (Moment magnitude), R_{rup} (Closest distance to rupture plane), ε (the difference between the spectral acceleration of a record and the mean of a ground motion prediction equation at the given period) and T_p (the pulse period

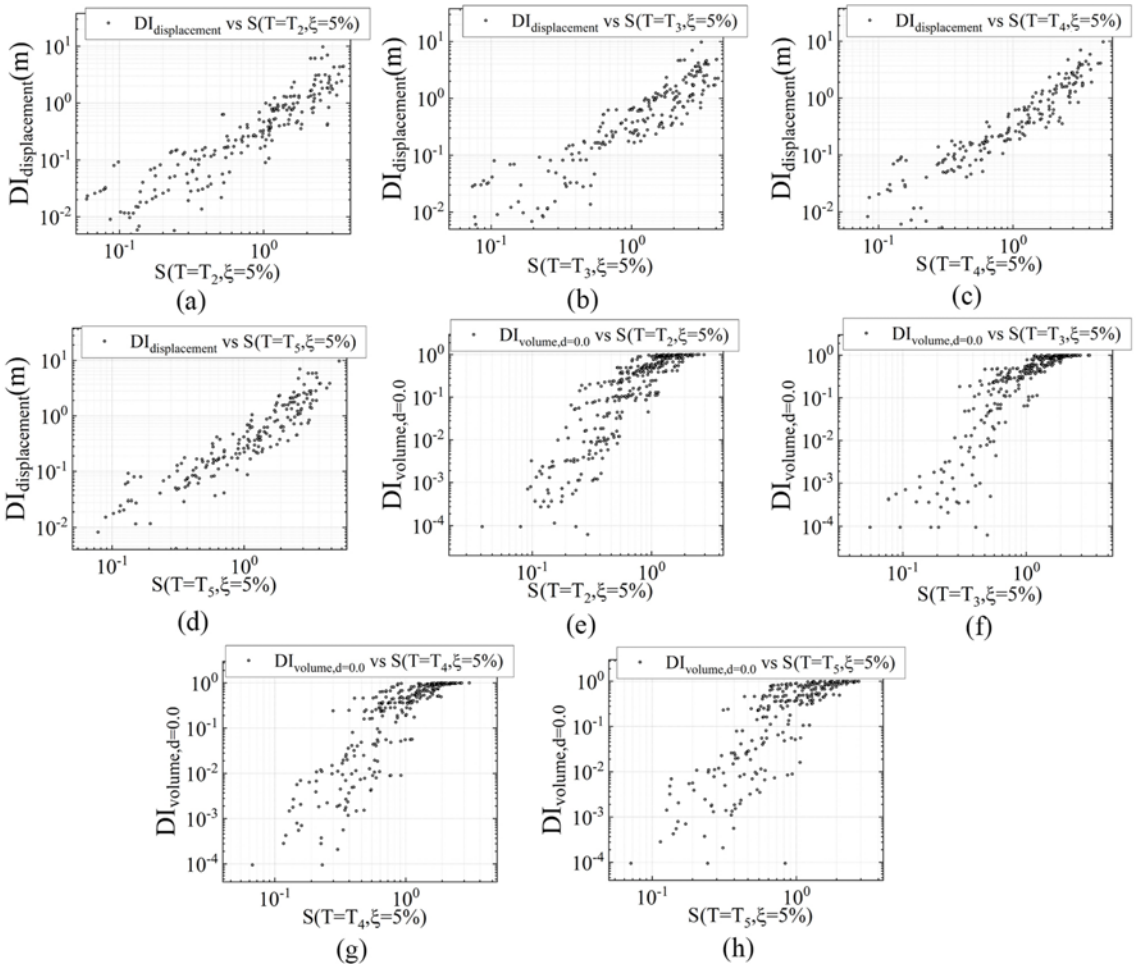

Fig. 8. EDPs-IMs Results in the Logarithmic Scale: (a) $DI_{displacement}$ vs. $S(T = T_2, \xi = 5\%)$, (b) $DI_{displacement}$ vs. $S(T = T_3, \xi = 5\%)$, (c) $DI_{displacement}$ vs. $S(T = T_4, \xi = 5\%)$, (d) $DI_{displacement}$ vs. $S(T = T_5, \xi = 5\%)$, (e) $DI_{volume,\ d=0.0}$ vs. $S(T = T_2, \xi = 5\%)$, (f) $DI_{volume,\ d=0.0}$ vs. $S(T = T_3, \xi = 5\%)$, (g) $DI_{volume,\ d=0.0}$ vs. $S(T = T_4, \xi = 5\%)$, (h) $DI_{volume,\ d=0.0}$ vs. $S(T = T_5, \xi = 5\%)$

Table 5. Demand Models and IM Comparisons for Displacement Response

No.	IM	b	β	ζ	R^2
1	CAV	1.00	0.53	0.53	0.88
2	EPA	1.56	0.61	0.39	0.87
3	EPA_{dam}	1.43	0.69	0.48	0.79
4	I_A	0.70	0.55	0.79	0.87
5	Ic	1.04	0.55	0.52	0.86
6	PGA	1.61	0.71	0.44	0.81
7	$S(T = T_1, \xi = 5\%)$	1.47	0.71	0.48	0.84
8	$S_a^{1\text{-to-}2}$	3.02	0.70	0.23	0.83
9	$S_a^{1\text{-to-}3}$	4.71	0.67	0.14	0.84
10	$S_a^{1\text{-to-}4}$	6.39	0.64	0.10	0.86
11	$S_a^{1\text{-to-}5}$	8.05	0.62	0.08	0.86
12	$S(T = T_2, \xi = 5\%)$	1.44	0.71	0.50	0.83
13	$S(T = T_3, \xi = 5\%)$	1.50	0.72	0.48	0.82
14	$S(T = T_4, \xi = 5\%)$	1.50	0.60	0.40	0.86
15	$S(T = T_5, \xi = 5\%)$	1.43	0.59	0.42	0.85
16	ASI	1.56	0.61	0.39	0.87

of the near-source record). Then linear regression between response residuals (ε^{EDP}|IM, the difference between the predicted value of lnEDP and the actual value when performing linear least-squares regression of lnEDP and IM_2 at the given IM_1; EDP, namely engineering demand parameter, in this paper, referred to seismic damage indices) and spectrum accelerations with different modes is performed to calculate the p-values, which represent the probability of rejecting the zero hypothesis and thus prove independency of this IM to other IMs. Higher p-value means this IM is more sufficient. Tables 6 – 9 reports the corresponding p-values on different structural response and spectrum accelerations with different modes. A 5% significance level can be selected as the criteria to reject the zero hypothesis in this study. Note that the data separated by vertical line in these tables are the p-values with damage level greater than 0.0, 0.3 and 0.5 respectively from left to right.

From Tables 6 and 9, all IMs are mutually non-independent for displacement and damage area ratio of downstream face (because all p-values are very small, far less than 0.05). Table 7 shows that for damage volume ratios of the dam body, PGA and

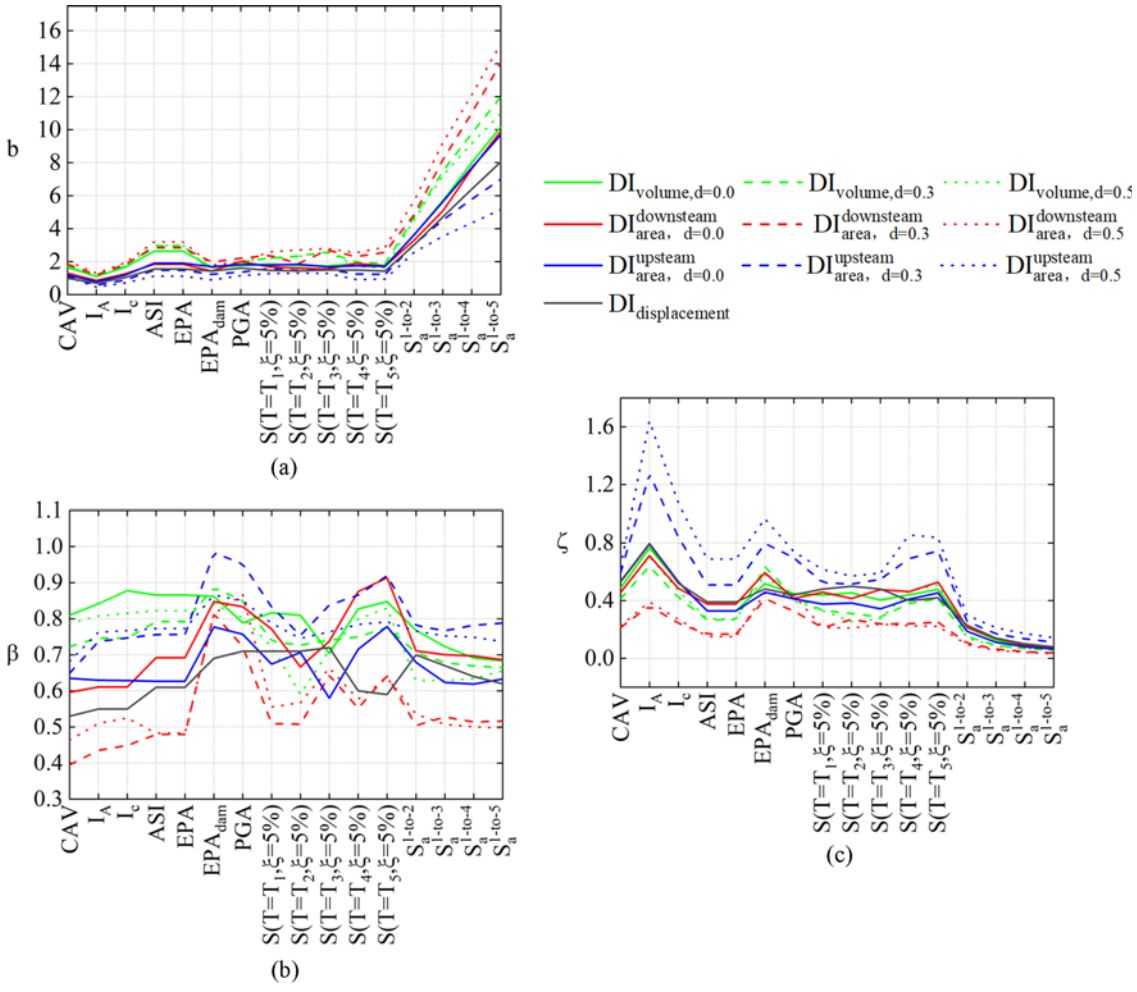

Fig. 9. PSDM's Parameters Based on Different Seismic Damage Indices: (a) Practicality, (b) Efficiency, (c) Proficiency

Table 6. The *p*-Values Based on Displacement

IM_1 \ IM_2 (*p*-value)	$S(T=T_1, \xi=5\%)$	$S(T=T_2, \xi=5\%)$	$S(T=T_3, \xi=5\%)$	$S(T=T_4, \xi=5\%)$	$S(T=T_5, \xi=5\%)$
PGA	0.000	0.000	0.000	0.000	0.000
$S(T=T_1, \xi=5\%)$	—	0.000	0.000	0.000	0.000
$S(T=T_2, \xi=5\%)$	—	—	0.000	0.000	0.000
$S(T=T_3, \xi=5\%)$	—	—	—	0.000	0.000
$S(T=T_4, \xi=5\%)$	—	—	—	—	0.000

$S(T=T_3, \xi=5\%)$, $S(T=T_1, \xi=5\%)$ and $S(T=T_5, \xi=5\%)$, $S(T=T_2, \xi=5\%)$ and $S(T=T_4, \xi=5\%)$, $S(T=T_5, \xi=5\%)$, $S(T=T_4, \xi=5\%)$ and $S(T=T_5, \xi=5\%)$ are not independent of each other when damage level is greater than 0.0, while PGA and $S(T=T_1, \xi=5\%)$, $S(T=T_2, \xi=5\%)$, $S(T=T_3, \xi=5\%)$, $S(T=T_4, \xi=5\%)$, $S(T=T_5, \xi=5\%)$, $S(T=T_3, \xi=5\%)$ and $S(T=T_4, \xi=5\%)$, $S(T=T_5, \xi=5\%)$ are not independent of each other when damage level is greater than 0.3 and 0.5. Again, based on Table 8, for damage area ratios of upstream face, all IMs are independent of each other when damage level is greater than 0.0 and 0.3 except that $S(T=T_2, \xi=5\%)$ is dependent of $S(T=T_3, \xi=5\%)$, $S(T=T_4, \xi=5\%)$ and $S(T=T_5, \xi=5\%)$ when damage level is greater than 0.3; $S(T=T_1, \xi=5\%)$ is independent of $S(T=T_2, \xi=5\%)$ and $S(T=T_3, \xi=5\%)$ when damage level is greater than 0.5.

Considering that for the arch dam, the structural response is affected by multi-order modes and different types of responses have significant differences, even the same IM based on different types of structural response is qualified by different *p*-values, and the IM alone can not fully reflect the correlation between structural responses and IMs. Therefore, when selecting the

Table 7. The *p*-Values Based on Damage Volume Rate for Dam Body

IM_1 \ IM_2 (*p*-value)	$S(T = T_1, \xi = 5\%)$	$S(T = T_2, \xi = 5\%)$	$S(T = T_3, \xi = 5\%)$	$S(T = T_4, \xi = 5\%)$	$S(T = T_5, \xi = 5\%)$
PGA	0.213|0.000|0.000	0.104|0.000|0.000	0.020|0.000|0.011	0.319|0.000|0.017	0.473|0.000|0.051
$S(T = T_1, \xi = 5\%)$	—	0.111|0.229|0.005	0.662|0.502|0.173	0.051|0.141|0.055	0.030|0.067|0.016
$S(T = T_2, \xi = 5\%)$	—	—	0.111|0.443|0.495	0.001|0.232|0.604	0.000|0.074|0.196
$S(T = T_3, \xi = 5\%)$	—	—	—	0.427|0.003|0.136	0.671|0.001|0.088

Table 8. The *p*-Values Based on Damage area Rate of Upstream Face

IM_1 \ IM_2 (*p*-value)	$S(T = T_1, \xi = 5\%)$	$S(T = T_2, \xi = 5\%)$	$S(T = T_3, \xi = 5\%)$	$S(T = T_4, \xi = 5\%)$	$S(T = T_5, \xi = 5\%)$
PGA	0.000|0.004|0.238	0.000|0.000|0.056	0.000|0.001|0.079	0.000|0.001|0.126	0.000|0.004|0.278
$S(T = T_1, \xi = 5\%)$	—	0.000|0.001|0.005	0.000|0.001|0.030	0.000|0.005|0.074	0.000|0.005|0.053
$S(T = T_2, \xi = 5\%)$	—	—	0.000|0.100|0.996	0.000|0.054|0.884	0.000|0.316|0.575
$S(T = T_3, \xi = 5\%)$	—	—	—	0.000|0.000|0.061	0.000|0.000|0.052
$S(T = T_4, \xi = 5\%)$	—	—	—	—	0.000|0.001|0.211

Table 9. The *p*-Values Based on Damage Area Rate of Downstream Face

IM_1 \ IM_2 (*p*-value)	$S(T = T_1, \xi = 5\%)$	$S(T = T_2, \xi = 5\%)$	$S(T = T_3, \xi = 5\%)$	$S(T = T_4, \xi = 5\%)$	$S(T = T_5, \xi = 5\%)$
PGA	0.000|0.000|0.000	0.000|0.000|0.000	0.000|0.000|0.000	0.000|0.000|0.001	0.000|0.000|0.000
$S(T = T_1, \xi = 5\%)$	—	0.000|0.000|0.000	0.000|0.000|0.000	0.000|0.000|0.000	0.000|0.000|0.000
$S(T = T_2, \xi = 5\%)$	—	—	0.000|0.003|0.000	0.001|0.002|0.000	0.000|0.000|0.000
$S(T = T_3, \xi = 5\%)$	—	—	—	0.000|0.000|0.000	0.000|0.000|0.000
$S(T = T_4, \xi = 5\%)$	—	—	—	—	0.000|0.000|0.000

optimal IM for different types of structural responses, one should pay attention to the influence of other IMs (mainly referring to the spectral acceleration with different modes here). Also, the rationality of the combined acceleration response spectra is testified here because these IMs include more information about the ground motion than PGA and spectrum accelerations with a specific vibration period alone.

5. Conclusions

In the present paper, ETAM is further applied to establish the relationship between structural response and IMs and to demonstrate the sufficiency of IMs reflecting the structural response of arch dams. Under the framework of ETAM, the evolution of damage-dependent DIs of arch dams under different damage levels is statistically analyzed. Then, the correlation between 16 ETA-related IMs and structural response of high arch dams in damage development stage is studied, and the sufficiency of each IM to the structural response of high arch dams is demonstrated. The results showed that:

1. Compared with the displacement-dependent DIs, performence status of arch dam can be clearly divided into three stages through the damage-dependent DIs, which can better reflect the evolution of structural response. And the practicality of IMs to the damage-dependent DIs is generally stronger than that of the displacement-dependent DIs, although the corresponding deviation is larger. Further, it is also seen that the upstream damage area ratio slightly has higher proficiency than the downstream damage area ratio under lower damage level ($d_t = 0.0$), but the result is the opposite under higher damage level ($d_t = 0.3$ and $d_t = 0.5$).
2. Note that ETAFs are generated from the response spectra of real ground motion records, so the variability of ETA results mainly comes from the variability of ETA target spectra, and is also affected by the process and method of ETAF generation. According to statistical analysis, the damage area ratio of the upstream surface of the arch dam is more discrete than other damage-dependent DIs. For the damage-dependent DIs' slopes in the damage development stage, the damage area ratio of the downstream surface has a higher slope at the lower damage level, while the slope of the each damage-dependent DI has little difference at higher damage level.
3. Based on the proficiency, combined spectral accelerations have the smallest ζ, and the value of ζ decreases with the higher combined modes; ASI and EPA have a smaller ζ

than spectral acceleration with a certain characteristic period of the structure; while for I_c, I_A and CAV, the value of ζ is larger than that of other IMs. Therefore, it is concluded that among the ETA-related IMs, the combined spectral acceleration $S_a^{1\text{-}to\text{-}N}$ is the most practical and proficient, and the more the number of combined modes increases, the more practical and proficient. ASI and EPA also show a good correlation with structural response of arch dam, which fully demonstrates that the structural response of arch dam is affected by high-order modes, and the seismic intensity parameters considering structural multi-order modes are obviously superior. However, the spectral acceleration with a specific vibration period have no obvious superiority because they can not consider the effect of structural multi-modal modes. Since I_c, I_A and CAV can not take into account the characteristics of the structure, they appear to be worse than other IMs.

4. It is also found that for different types of structural responses, the performance of IMs is different, and the IM alone can not fully reflect the structural response. This fully demonstrates that when establishing the relationship between structural response and IMs, the correlation among IMs based on structural response should be fully demonstrated in order to predict the structural response in performance-based seismic engineering with more sufficient IM.

Acknowledgments

This research is financially supported by the National Key Research and Development Plan (Grant No. 2017YFC0404900) and the National Natural Science Foundation of China (Grant No. 51679030). The authors express heartfelt thanks to the support.

ORCID

Not Applicable

References

Abrahamson NA, Silva WJ (1997) Empirical response spectral attenuation relations for shallow crustal earthquakes. *Seismological Research Letters* 68(1):94-127, DOI: 10.1785/gssrl.68.1.94

Alavi B, Krawinkler H (2001) Effects of near-fault ground motions on frame structures. Report No. 138, John A. Blume Earthquake Engineering Center, Stanford University, Stanford, CA, USA

Ang A (1990) Reliability bases for seismic safety assessment and design. Proceedings of the fourth US national conference on earthquake engineering, May 20-24, Palm Springs, CA, USA

Arias A (1970) A measure of earthquake intensity. In: Hansen RJ (ed) Seismic design for nuclear power plants, The MIT Press, Cambridge, MA, USA, 438-483

BSSC (1984) NEHRP recommended provisions for the development of seismic regulations for new buildings. Building Seismic Safety Council, Federal Emergency Management Agency, Washington DC, USA

Buffi G, Manciola P, de LorenzisL, Cavalagli N, Comodini F, Gambi A, Gusella V, Mezzi M, Niemeier W, Tamagnini C (2017) Calibration of finite element models of concrete arch-gravity dams using dynamical measures: The case of Ridracoli. *Procedia Engineering* 199:110-115, DOI: 10.1016/j.proeng.2017.09.169

Camara RJ (2000) A method for coupled arch dam-foundation-reservoir seismic behaviour analysis. *Earthquake Engineering and Structural Dynamics* 29(4):441-460, DOI: 10.1002/(SICI)1096-9845(200004)29:4<441::AID-EQE916>3.0.CO;2-B

Chen JY, Cao XY, Xu Q, Li J (2020a) Exploration on damage mechanism and equivalent damage model of high arch dams under earthquakes. *KSCE Journal of Civil Engineering* 24(4):1285-1306, DOI: 10.1007/s12205-020-1267-8

Chen JY, Qin LJ, Xu Q, Li J (2020b) Seismic damage indexes of a high arch dam based on the monolith. *KSCE Journal of Civil Engineering* 24(7):2078-2087, DOI: 10.1007/s12205-020-1202-z

Chen H, Wu S, Dang F (2012) Seismic safety of high arch dams. China Electric Power Press, Beijing, China, 35-39

Cornell CA, Jalayer F, Hamburger RO, Foutch DA (2002) Probabilistic basis for 2000 SAC federal emergency management agency steel moment frame guidelines. *Journal of Structural Engineering* 128(4):526-533, DOI: 10.1061/(ASCE)0733-9445(2002)128:4(526)

Estekanchi HE, Alembagheri M (2012) Seismic analysis of steel liquid storage tanks by endurance time method. *Thin-Walled Structures* 50(1):14-23, DOI: 10.1016/j.tws.2011.08.015

Estekanchi HE, Riahi HT, Vafai A (2011) Application of endurance time method in seismic assessment of steel frames. *Engineering Structures* 33(9):2535-2546, DOI: 10.1016/j.engstruct.2011.04.025

Estekanchi HE, Vafai A, Sadeghazar M (2004) Endurance time method for seismic analysis and design of structures. *Scientia Iranica* 11(4):361-370

Estekanchi HE, Valamanesh V, Vafai A (2007) Application of endurance time method in linear seismic analysis. *Engineering Structures* 29(10):2551-2562, DOI: 10.1016/j.engstruct.2007.01.009

Furgani L, Meghella M (2015) Endurance time analysis for the seismic vulnerability of arch dams. Proceedings of the 13th ICOLD benchmark workshop on numerical analysis of dams, Swiss Committee on Dams, Lausanne, Switzerland

Garcia-Mayordomo J, Insua-Arevalo JM (2011) Seismic hazard assessment for the Itoiz dam site (Western Pyrenees, Spain). *Soil Dynamics and Earthquake Engineering* 31(7):1051-1063, DOI: 10.1016/j.soildyn.2011.03.011

Guo AX, Shen Y, Bai JL, Li H (2017) Application of the endurance time method to the seismic analysis and evaluation of highway bridges considering pounding effects. *Engineering Structures* 131:220-230, DOI: 10.1016/j.engstruct.2016.11.009

Hariri-Ardebili MA, Furgani L, Meghella M, Saouma V (2016) A new class of seismic damage and performance indices for arch dams via ETA method. *Engineering Structures* 110:145-160, DOI: 10.1016/j.engstruct.2015.11.021

Hariri Ardebili MA, Mirzabozorg H (2011) Investigation of endurance time method capability in the seismic performance evaluation of concrete arch dams. *Dam Engineering* 22(1):35

Hariri-Ardebili MA, Mirzabozorg H (2014) Estimation of probable damages in arch dams subjected to strong ground motions using endurance time acceleration functions. *KSCE Journal of Civil Engineering* 18(3):574-586, DOI: 10.1007/s12205-013-0264-6

Hariri-Ardebili MA, Mirzabozorg H, Estekanchi HE (2014) Nonlinear seismic assessment of arch dams and investigation of joint behavior using endurance time analysis method. *Arabian Journal for Science*

and Engineering 39(5):3599-3615, DOI: 10.1007/s13369-014-1027-5

Hariri-Ardebili MA, Saouma VE (2016a) Collapse fragility curves for concrete dams: Comprehensive study. *Journal of Structural Engineering* 142(10):04016075, DOI: 10.1061/(asce)st.1943-541x.0001541

Hariri-Ardebili MA, Saouma VE (2016b) Probabilistic seismic demand model and optimal intensity measure for concrete dams. *Structural Safety* 59:67-85, DOI: 10.1016/j.strusafe.2015.12.001

Hariri-Ardebili MA, Saouma VE (2016c) Seismic fragility analysis of concrete dams: A state-of-the-art review. *Engineering Structures* 128:374-399, DOI: 10.1016/j.engstruct.2016.09.034

Kostinakis K, Fontara IK, Athanatopoulou AM (2018) Scalar structure-specific ground motion intensity measures for assessing the seismic performance of structures: A review. *Journal of Earthquake Engineering* 22(4):630-665, DOI: 10.1080/13632469.2016.1264323

Kramer SL (1996) Geotechnical earthquake engineering. Prentice Hall, Englewood Cliffs, NJ, USA

Kuo JS-H (1982) Fluid-structure interactions: Added mass computations for incompressible fluid. University of California, College of Engineering, Earthquake Engineering Research Center, Berkeley, CA, USA

Lee J, Fenves GL (1998) Plastic-damage model for cyclic loading of concrete structures. *Journal of Engineering Mechanics* 124(8):892-900, DOI: 10.1061/(asce)0733-9399(1998)124:8(892)

Luco N, Cornell CA (2007) Structure-specific scalar intensity measures for near-source and ordinary earthquake ground motions. *Earthquake Spectra* 23(2):357-392, DOI: 10.1193/1.2723158

MATLAB® 9.1.0 (2016) The Mathworks Inc, Retrieved October 9, 2019, https://www.mathworks.com/

Meghella M, Furgani L (2014) Application of endurance time analysis method to the nonlinear seismic analysis of dams: Potentialities and limitations. Proceedings of the 82nd annual meeting of ICOLD, Banff, AB, Canada

Mehanny SS (2009) A broad-range power-law form scalar-based seismic intensity measure. *Engineering Structures* 31(7):1354-1368, DOI: 10.1016/j.engstruct.2009.02.003

Mirzabozorg H, Kordzadeh A, Hariri-Ardebili MA (2012) Seismic response of concrete arch dams including dam-reservoir-foundation interaction using infinite elements. *Electronic Journal of Structural Engineering* 12(1)

National Energy Administration of China (2015) Code for seismic design of hydraulic structures of hydropower project NB 35047-2015. China Electric Power Press, Beijing, China

Nozari A, Estekanchi HE (2011) Optimization of endurance time acceleration functions for seismic assessment of structures. *International Journal of Optimization in Civil Engineering* 1(2):257-277

Omidi O, Lotfi V (2017) Seismic plastic–damage analysis of mass concrete blocks in arch dams including contraction and peripheral joints. *Soil Dynamics and Earthquake Engineering* 95:118-137, DOI: 10.1016/j.soildyn.2017.01.026

Pacific Earthquake Engineering Research Center (2013) PEER ground motion database. Retrieved September 15, 2018, http://ngawest2.berkeley.edu/site/

Padgett JE, Nielson BG, DesRoches R (2008) Selection of optimal intensity measures in probabilistic seismic demand models of highway bridge portfolios. *Earthquake engineering and structural dynamics* 37(5):711-725, DOI: 10.1002/eqe.782

Pan JW, Zhang CH, Wang JT, Xu YJ (2009) Seismic damage-cracking analysis of arch dams using different earthquake input mechanisms. *Science in China Series E: Technological Sciences* 52(2):518-529, DOI: 10.1007/s11431-008-0303-6

Razali NM, Wah YB (2011) Power comparisons of Shapiro-Wilk, Kolmogorov-Smirnov, Lilliefors and Anderson-Darling tests. *Journal of Statistical Modeling and Analytics* 2(1):21-33

Riahi HT, Estekanchi HE, Vafai A (2009) Endurance time method-application in nonlinear seismic analysis of single degree of freedom systems. *Journal of Applied Sciences* 9(10):1817-1832, DOI: 10.3923/jas.2009.1817.1832

Salamon JW, Hariri-Ardebili MA, Estekanchi HE, Mashayekhi MR (2019) Seismic assessment of a dam-foundation-reservoir system using Endurance Time Analysis. Proceedings of the ICOLD 2019 symposium, June 9-14, Ottawa, Canada

Simulia DS (2011) Abaqus 6.11 theory manual. DS SIMULIA Corp., Providence, RI, USA

Song ZQ, Wang F, Liu YJ, Su CH (2018) Infinite element static-dynamic unified artificial boundary. *Shock and Vibration* 2018, DOI: 10.1155/2018/7828267

Tavazo H, Estekanchi HE, Kaldi P (2012) Endurance time method in the linear seismic analysis of shell structures. *International Journal of Civil Engineering* 10(3):169-178

Valamanesh V, Estekanchi HE, Vafai A, Ghaemian M (2011) Application of the endurance time method in seismic analysis of concrete gravity dams. *Scientia Iranica* 18(3):326-337, DOI: 10.1016/j.scient.2011.05.039

von Thun JL, Rochim LH, Scott GA, Wilson JA (1988) Earthquake ground motions for design and analysis of dams. Earthquake engineering and soil dynamics II - Recent advances in ground-motion evaluation: Proceedings of the specialty conference, June 27-30, Park City, UT, USA

Wang JT, Jin AY, Du XL, Wu MX (2016) Scatter of dynamic response and damage of an arch dam subjected to artificial earthquake accelerograms. *Soil Dynamics and Earthquake Engineering* 87:93-100, DOI: 10.1016/j.soildyn.2016.05.003

Wang JT, Lv DD, Jin F, Zhang CH (2013a) Earthquake damage analysis of arch dams considering dam–water–foundation interaction. *Soil Dynamics and Earthquake Engineering* 49:64-74, DOI: 10.1016/j.soildyn.2013.02.006

Wang JT, Zhang CH, Jin F (2013b) Nonlinear earthquake analysis of high arch dam-water-foundation rock systems. *Seismic Safety Evaluation of Concrete Dams* 311-340, DOI: 10.1016/B978-0-12-408083-6.00014-3

Westergaard HM (1933) Water pressures on dams during earthquakes. *Transactions of the American Society of Civil Engineers* 95:418-433, DOI: 10.1016/S0016-0032(20)90373-3

Zacchei E, Molina JL (2020) Reviewing arch-dams' building risk reduction through a sustainability–safety management approach. *Sustainability* 12(1), DOI: 10.3390/su12010392

Zhang CH, Pan JW, Wang JT (2009) Influence of seismic input mechanisms and radiation damping on arch dam response. *Soil Dynamics and Earthquake Engineering* 29(9):1282-1293, DOI: 10.1016/j.soildyn.2009.03.003